



Published in final edited form as:

Leukemia. 2019 October ; 33(10): 2506–2521. doi:10.1038/s41375-019-0462-4.

Kdm6b Regulates Context-Dependent Hematopoietic Stem Cell Self-Renewal and Leukemogenesis

Cates Mallaney¹, Elizabeth L. Ostrander¹, Hamza Celik¹, Ashley C. Kramer¹, Andrew Martens¹, Alok Kothari², Won Kyun Koh¹, Emily Haussler¹, Naoki Iwamori³, Paul Gontarz⁴, Bo Zhang⁴, Grant A. Challen^{1,*}

¹Division of Oncology, Department of Medicine, Washington University School of Medicine, St. Louis, MO, USA, 63110.

²Department of Pediatrics, Washington University School of Medicine, St. Louis, MO, USA, 63110.

³Laboratory of Biomedicine, Division of Pathobiology, Department of Basic Medicine, Faculty of Medicine, Kyushu University, Fukuoka 812-8582, Japan

⁴Center of Regenerative Medicine, Department of Developmental Biology, Washington University School of Medicine, St. Louis, MO, USA, 63110.

Abstract

The histone demethylase KDM6B (JMJD3) is upregulated in blood disorders, suggesting it may have important pathogenic functions. Here we examined the function of *Kdm6b* in hematopoietic stem cells (HSC) to evaluate its potential as a therapeutic target. Loss of *Kdm6b* lead to depletion of phenotypic and functional HSCs in adult mice, and *Kdm6b* is necessary for HSC self-renewal in response to inflammatory and proliferative stress. Loss of *Kdm6b* leads to a pro-differentiation poised state in HSCs due to the increased expression of the AP-1 transcription factor complex (*Fos* and *Jun*) and immediate early response (IER) genes. These gene expression changes occurred independently of chromatin modifications. Targeting AP-1 restored function of *Kdm6b*-deficient HSCs, suggesting Kdm6b regulates this complex during HSC stress response. We also show *Kdm6b* supports developmental context-dependent leukemogenesis for T-cell acute lymphoblastic leukemia (T-ALL) and M5 acute myeloid leukemia (AML). *Kdm6b* is required for effective fetal-derived T-ALL and adult-derived AML, but not *vice versa*. These studies identify a crucial role for

Users may view, print, copy, and download text and data-mine the content in such documents, for the purposes of academic research, subject always to the full Conditions of use:http://www.nature.com/authors/editorial_policies/license.html#terms

*Corresponding author: Grant A. Challen, Ph.D., Washington University School of Medicine, 660 Euclid Avenue, St. Louis, MO, USA. 63110, Ph: +1 314-362-0987, gchallen@dom.wustl.edu.

AUTHOR CONTRIBUTIONS

Project conceptualization and experimental design: G.A.C.

Performed experiments: C.M., E.L.O., H.C., A.C.K., A.M., A.K., W.K.K., E.H., G.A.C.

Provided critical reagents: N.I.

Data analysis: C.M., E.L.O., P.G., B.Z., G.A.C.

Writing – original draft preparation: C.M.

Writing – review and editing: G.A.C.

Project administration and funding acquisition: G.A.C.

COMPETING INTERESTS

The authors declare no competing interests.

Kdm6b in regulating HSC self-renewal in different contexts, and highlight the potential of KDM6B as a therapeutic target in different hematopoietic malignancies.

Keywords

Hematopoietic stem cell; epigenetics; cancer stem cell; self-renewal; AP-1

INTRODUCTION

KDM6B (JMJD3) is one of two epigenetic modifiers responsible for enzymatic removal of the repressive chromatin mark histone H3 lysine 27 trimethylation (H3K27me3)¹. H3K27me3 is associated with transcriptional repression and gene silencing². Demethylation of H3K27me3 by either KDM6B or UTX1 (KDM6A) is required for resolution of bivalent chromatin domains, lineage-specific gene expression and differentiation in embryonic stem cells³⁻⁶. In somatic cells, KDM6B plays a role in stress response in macrophages⁷⁻⁹, hippocampal neurons¹⁰, and fibroblasts^{11, 12}, and may have demethylase-independent functions in response to different physiological perturbations^{7, 13}. However, most of these studies have been performed in cell lines. As these molecular functions of epigenetic regulators are highly cell type-dependent, analysis of purified populations is required to deconvolute specific activities in primary cells.

Genome sequencing of hematopoietic malignancies has identified somatic mutations in many epigenetic modifiers¹⁴⁻¹⁶. While *UTX1* mutations are recurrent in blood cancers^{16, 17}, *KDM6B* mutations have not been identified apart from chromosomal deletions in Sezary syndrome¹⁸. In contrast, *KDM6B* is over-expressed in a myriad of blood disorders including myelodysplastic syndromes (MDS)¹⁹, Hodgkin's lymphoma (HL)²⁰, multiple myeloma (MM)¹³, and T-cell acute lymphoblastic leukemia (T-ALL)²¹. KDM6B seems to have opposing roles in leukemia development dependent on morphological subtype and genetic background. While UTX1 acts as a tumor suppressor in *NOTCH1*-driven T-ALL, KDM6B supports this leukemia by activating oncogenic gene expression²¹. In contrast, KDM6B has oncorepressor activity M2/M3 AML (granulocytic subtypes). Downregulation of *KDM6B* in these AMLs results in differentiation arrest and correlates with poor clinical outcomes²². The role of KDM6B in hematopoietic development must be defined to understand the mechanisms through which it acts in different leukemia subtypes.

A recent study showed constitutive over-expression of *Kdm6b* in the hematopoietic system leads to upregulation of genes involved in innate immune signaling, resulting in compromised hematopoiesis and pathologies reminiscent of human MDS²³. But the function of Kdm6b specifically in hematopoietic stem cells (HSCs) has not been studied. Here, we developed a conditional genetic mouse model to study *Kdm6b* in hematopoietic development, HSC fate decisions and leukemogenesis. We show that loss of *Kdm6b* leads to the inability for HSCs to self-renew following proliferative stress, driven in part by H3K27me3-independent dysregulation of the AP-1 transcription factor complex. We also show that *Kdm6b* supports context-dependent leukemia initiation and maintenance, conditional upon disease subtype and developmental age.

METHODS

Mice and Transplantation

All animal procedures were approved by the Institutional Animal Care and Use Committee at Washington University. All mice were C57Bl/6 background. *Kdm6b^{fl/fl}* and *Utx^{fl/fl}* mice were crossed to Vav-CRE²⁶, Mx1-CRE²⁷ or ERT2-CRE²⁸ strains. Six doses (300 µg/mouse) of polyinosinic:polycytidylic acid (pIpC; Sigma #p1530) were administered every other day via intraperitoneal injection to induce Mx1-CRE. Nine doses (4 mg) of Tamoxifen (Sigma #T5648) in corn oil (Sigma #C8267) were administered via oral gavage to induce ERT2-CRE. For transplantation, recipient mice (CD45.1) were given a split dose (~4-hours apart) of lethal irradiation (10.5 Gy). For secondary leukemia transplants, recipient mice were given a sublethal dose (6.0 Gy) of irradiation.

Flow Cytometry

Samples were incubated at 4°C for >20 minutes with appropriate antibodies. Bone marrow was enriched with anti-mouse CD117-conjugated microbeads (Miltenyi Biotec #130-091-224) prior to HSC purification. Donor cell chimerism (CD45.1 vs. CD45.2) and lineage contribution was determined by assessing myeloid (Gr-1+ Mac-1+), B-cell (B220+) and T-cell (CD3e+) populations in peripheral blood. For intracellular flow cytometry, samples were stained for surface markers overnight at 4°C, processed using the Cytotfix/Cytoperm Kit (BD Biosciences #554714), then stained with intracellular antibodies for 20 minutes at room temperature.

Plasmids and Viral Transduction

293T (ATCC #CRL-3216) cells were co-transfected with packaging vector (pCL-Eco) and either empty vector control (MIG-GFP), MIG-NICD or MIG-MLL-AF9 using Lipofectamine 3000 (ThermoFisher Scientific #L3000008). 1.0×10^6 cells/500µL were plated in Stempro-34 medium (Gibco #10639011) supplemented with Pen-Strep (100 Units/mL), L-glutamine (2 mM), mSCF (100 ng/mL), mTPO (100ng/mL), mFlt3L (50ng/mL), mIL-3 (5 ng/mL), and polybrene (4 µg/mL; Sigma), and spininfected with retrovirus supernatant at 250g for two-hours.

RNA-SEQ

RNA was isolated using the NucleoSpin RNA XS kit (Macherey-Nagel #740902.250). The SMARTer Ultra Low RNA kit (Clontech) was used to prepare libraries. Sequencing was performed with an Illumina HiSeq-3000. RNA-seq reads were aligned to the Ensembl release 76 top-level assembly with STAR version 2.0.4b²⁹. Gene counts were derived from the number of uniquely aligned reads by Subread:featureCount version 1.4.5^{30, 31}. Transcript counts were generated by Sailfish version 0.6.3³². Gene set enrichment analysis (GSEA)³³ was performed to identify dysregulated genesets. Primary data is available under GEO accession number GSE110378.

ChIP-mentation

ChIP-mentation was performed as previously described³⁴. Chromatin was sheared using a Covaris E220 Focused-ultrasonicator and incubated overnight at 4°C with H3K27me3 antibody (Diagenode #pAb-069-050) or H3K4me3 antibody (Diagenode #pAb-003-050). Libraries were sequenced on an Illumina Hiseq 3000. Sequences were aligned to mm10 using Bowtie2³⁵. Peak calling was performed with hiddenDomains³⁶, the R package ChIPQC³⁷ was used for quality control including PCA plots. HOMER plots for H3K27me3 and H3K4me3 were made using deepTools³⁸. BEDOPS³⁹ was used to determine overlapping and unique peaks. Primary data is available under GEO accession number GSE110378.

ATAC-seq

Using a modified Omni-ATAC method⁴⁰, 10,000 HSCs were sorted and the transposition reaction was carried out in 2x TD/Transposase buffer with transposase (Nextera) for 30 minutes at 37°C. Libraries were generated using NEBnext (NewEngland Biolabs) and run on an Illumina Hiseq 3000. Primary data is available under GEO accession number GSE110378.

Statistics

Student t-test, one-way, and two-way ANOVA's were used for statistical comparisons where appropriate. Survival curves were analyzed using a Mantel-Cox logrank test. Significance is indicated using the following convention: * $p < 0.05$, ** $p < 0.01$, *** $p < 0.001$, **** $p < 0.0001$. All graphs represent mean \pm S.E.M.

RESULTS

Loss of Kdm6b results in depletion of primitive hematopoietic progenitors

A conditional knockout mouse was generated by crossing the Vav-CRE driver²⁶ to delete floxed exons 14–20²⁴ of *Kdm6b* in hematopoietic cells. Complete floxed allele recombination was observed in HSCs (Lineage- Sca-1+ c-Kit+ CD48- CD150+ EPCR+; Supplementary Figure 1a). Complete protein ablation was observed in thymocytes (Supplementary Figure 1b), but global H3K27me3 was unchanged (Supplementary Figure 1c). Whole bone marrow (WBM) cellularity (Supplementary Figure 1d) and spleen weight (Supplementary Figure 1e) were unchanged in young adult (eight-week old) Vav-CRE:*Kdm6b*^{fl/+} (*Kdm6b*-Het^{VAV}) and Vav-CRE:*Kdm6b*^{fl/fl} (*Kdm6b*-KO^{VAV}) mice. Both heterozygous- and homozygous mice showed increased B-cells and reduced myeloid cells in the blood (Supplementary Figure 1f) compared to control mice (Vav-CRE:*Kdm6b*^{+/+} = Control^{Vav}). No hematological disease was observed in mutant mice by 80-weeks of age and blood counts remained relatively normal (Supplementary Figure 1g–k).

Flow cytometry analysis (Figure 1a) revealed slightly reduced frequency and absolute number of HSCs and multipotent progenitor cell (MPPs; Lineage- EPCR+ c-Kit+ Sca-1+ CD48- CD150-) in young adult *Kdm6b*-KO^{VAV} mice (Figure 1b). This depletion of HSCs and MPPs was magnified in aged mice (Figure 1c). Colony-forming units were reduced in *Kdm6b*-KO^{VAV} WBM (Figure 1d) and serial replating of purified heterozygous- and

homozygous HSCs was defective (Figure 1e). Detailed analysis revealed minimal differences in myeloid (Supplementary Figure 2a–c), lymphoid (Supplementary Figure 2d–f), B-cell (Supplementary Figure 2g–i) and erythroid (Supplementary Figure 2j–l) progenitors with age. In agreement with previous studies⁴¹, there was increased CD4+ and CD8a+ cells in the thymus of *Kdm6b*-KO^{VAV} mice (Supplementary Figure 2m–o).

Kdm6b is required for HSC self-renewal

To determine if loss of phenotypic HSCs in *Kdm6b*-KO^{VAV} mice correlated with functional decline, limiting dilutions of WBM from Control^{VAV}, *Kdm6b*-Het^{VAV} and *Kdm6b*-KO^{VAV} mice were competitively transplanted. Recipients were classified as long-term multi-lineage reconstituted (LTMR) if B-cell, T-cell and myeloid blood lineages had >1% donor-derived engraftment at 16-weeks post-transplant (Figure 2a). The proportion of LTMR mice at each dose was used to calculate long-term repopulating cell frequency⁴². While Control^{VAV} and *Kdm6b*-Het^{VAV} mice had a comparable frequency of long-term repopulating cells (1:49,984 and 1:55,422 respectively), *Kdm6b*-KO^{VAV} WBM was estimated to have a two-fold reduction (1:108,101; $p=0.054$, Figure 2b). *Kdm6b*-KO^{VAV} HSCs were reduced in recipient mice 18-weeks post-transplant (Figure 2c). To assess self-renewal, 3.0×10^6 WBM from LTMR mice was transferred to secondary recipients. *Kdm6b*-KO^{VAV} secondary recipients had no long-term engraftment (Figure 2d). While overall engraftment was equivalent between Control^{VAV} and *Kdm6b*-Het^{VAV} recipients, only 37.5% of *Kdm6b*-Het^{VAV} recipient mice were LTMR compared to 83.3% of Control^{VAV} recipients (Figure 2e). Post-secondary transplant, *Kdm6b*-Het^{VAV} HSCs were reduced in recipient bone marrow (Figure 2f).

To examine Kdm6b function specifically in HSCs, 200 HSCs were purified from Control^{VAV}, *Kdm6b*-Het^{VAV} and *Kdm6b*-KO^{VAV} mice and competitively transplanted. While initial engraftment was comparable, subsequent timepoints showed significantly decreased contribution from *Kdm6b*-KO^{VAV} HSCs (Figure 2g). *Kdm6b*-Het^{VAV} and *Kdm6b*-KO^{VAV} HSCs contributed equally to all three blood lineages (Figure 2h). 18-weeks post-transplant, 200 HSCs from primary recipients were re-purified and transplanted into secondary recipients. The severe reduction in donor-derived HSCs (Figure 2i) in *Kdm6b*-KO^{VAV} recipients precluded secondary transfer. Secondary transplant saw a mild reduction in donor-derived chimerism in *Kdm6b*-Het^{VAV} recipients (Supplementary Figure 3a) across all blood lineages (Supplementary Figure 3b), but post-secondary transplant there was a significant reduction in *Kdm6b*-Het^{VAV} donor-derived HSCs (Supplementary Figure 3c). The engraftment deficiency from *Kdm6b*-mutant mice could not be attributed to homing defects (Supplementary Figure 3d). To examine effect of age, 5.0×10^5 WBM from old (80-week) Control^{VAV}, *Kdm6b*-Het^{VAV}, or *Kdm6b*-KO^{VAV} mice was transplanted with 2.5×10^5 wild-type WBM competitor cells. Aged WBM from *Kdm6b*-Het^{VAV} and *Kdm6b*-KO^{VAV} mice showed a significant reduction in blood chimerism (Figure 2j), lymphoid engraftment (Figure 2k), and HSC regeneration (Figure 2l).

Kdm6b loss leads to a stress response gene expression signature in HSCs independent of chromatin changes

To elucidate mechanisms underlying self-renewal defect of *Kdm6b*-KO^{VAV} HSCs, global transcriptomic analysis was performed. Comparison of RNA-seq profiles of Control^{VAV} and

Kdm6b-KO^{VAV} HSCs to define genes with >2-fold increased or decreased expression (adjusted *p*-value <0.05) identified 649 genes (Supplementary Table 1). The majority (88.3%) of these genes showed increased expression in *Kdm6b*-KO^{VAV} HSCs (Figure 3a). Gene Set Enrichment Analysis (GSEA) identified several inflammatory response pathways upregulated in *Kdm6b*-KO^{VAV} HSCs (Supplementary Figure 4a). The expression profile of *Kdm6b*-KO^{VAV} HSCs overlapped with genesets enriched in aged HSCs ($p=3.8655\times 10^{-8}$)⁴³ and immediate early response (IER) genes ($p=1.6495\times 10^{-9}$)⁴⁴. Genes downregulated in HSCs in response to 5-Fluorouracil (5-FU)⁴⁵ were significantly upregulated in *Kdm6b*-KO^{VAV} HSCs ($p=0.000295$; Figure 3b), suggesting loss of *Kdm6b* results in a state whereby HSCs are primed for differentiation. Of the overlapping genes, the IER master transcription factor AP-1 subunits *Jun* and *Fos* were consistently identified (Figure 3b).

ChIP-mentation³⁴ for H3K27me3 and H3K4me3 was performed on Control^{VAV} and *Kdm6b*-KO^{VAV} HSCs to determine if gene expression differences were associated with chromatin changes. H3K4me3 peaks were highly overlapping (Supplementary Figure 4b) with 99.98% of the 16,163 peaks within 5kB of a transcriptional start site conserved between Control^{VAV} and *Kdm6b*-KO^{VAV} HSCs (Supplementary Figure 4c–e). Similarly, of the 6,232 H3K27me3 domains within 5kB of a transcriptional start site, 99.94% were conserved between genotypes (Figure 3c). No differentially expressed genes in *Kdm6b*-KO^{VAV} HSCs were associated with changes in chromatin methylation (Figure 3d,e), exemplified by *Fos* and *Jun* (Figure 3f). ATAC-seq was performed on Control^{VAV} and *Kdm6b*-KO^{VAV} HSCs, but there were also minimal differences in chromatin accessibility with only 1,305 peaks enriched in Control^{VAV} HSCs compared to 91,276 total peaks (1.43%; Supplementary Figure 4f). Similarly, only 1,688/81,203 ATAC-seq peaks (2.08%) were enriched in *Kdm6b*-KO^{VAV} HSCs (Supplementary Figure 4g; Supplementary Table 2). Interestingly, one of the few loci that showed a change in chromatin accessibility in *Kdm6b*-KO^{VAV} HSCs encompassed *Fos* (Figure 3g). The *Jun* locus also appeared more open in *Kdm6b*-KO^{VAV} HSCs although not statistically significant (Figure 3g). But like other results, the open chromatin at these loci in the mutant HSCs was not associated with increased marks of active chromatin like H3K9ac and H3K27ac (Figure 3g).

Inflammatory stress rapidly depletes *Kdm6b*-deficient HSCs

Gene expression analysis of *Kdm6b*-KO^{VAV} HSCs enlightened a previous result. To initially study *Kdm6b* in HSCs, *Kdm6b*^{fl/fl} mice were crossed to the Mx1-CRE driver²⁷. Mx1-CRE is induced in hematopoietic cells by polyinosinic:polycytidylic (pIpC) acid, an immunostimulant that elicits an IFN α response⁴⁶. Mx1-CRE:*Kdm6b*^{+/+} (Control^{MX1}), Mx1-CRE:*Kdm6b*^{fl/+} (*Kdm6b*-Het^{MX1}), and Mx1-CRE:*Kdm6b*^{fl/fl} (*Kdm6b*-KO^{MX1}) mice were treated with six-doses of pIpC, allowed to recover for six-weeks, then 200 HSCs were competitively transplanted. *Kdm6b*-KO^{MX1} HSCs showed severely compromised engraftment (Figure 4a) and HSC regeneration (Figure 4b). At the time of transplant, individual HSCs were concurrently sorted to determine floxing efficiency. 56.9% of *Kdm6b*-KO^{MX1} HSCs retained both floxed alleles, and only 22.3% of HSCs had deletion of both *Kdm6b* alleles (Figure 4c). While efficiency of recombination in *Kdm6b*-Het^{MX1} HSCs was higher, 30.5% were still intact (Figure 4c). To determine if this CRE-deficiency was specific to the *Kdm6b* allele, floxing efficiency of Mx1-CRE:*Utx*^{fl/+} (*Utx*-Het^{MX1}) HSCs was

assessed²⁵. Only 9.1% of *Utx1*-Het^{MX1} HSCs were not recombined six-weeks post-pIpC (Figure 4c). Post-transplant, only 10.8% of *Kdm6b*-Het^{MX1} HSCs retained unrecombined alleles (Figure 4c). We were unable to recover *Kdm6b*-KO^{MX1} HSCs post-transplant to assess floxing efficiency. While primary *Kdm6b*-Het^{MX1} recipients showed no engraftment defects, secondary transplantation showed a significant decrease (Figure 4d). 18-weeks post-secondary transplant, donor-derived HSCs were virtually undetectable in *Kdm6b*-Het^{MX1} recipients (Figure 4e).

To determine why *Kdm6b*-deficient HSCs were rapidly depleted in response to pIpC, 200 HSCs from untreated Mx1-CRE:*Kdm6b*^{+/+} and Mx1-CRE:*Kdm6b*^{fl/fl} mice were transplanted, then treated with pIpC four-weeks post-transplant. Granulocytes were purified from donor mice pre-transplant, and compared to donor-derived granulocytes from recipient mice to examine floxing efficiency. As granulocytes have a very short half-life, their generation reflects the output of active HSCs. Analysis of genomic DNA indicated granulocytes two-weeks post-pIpC were derived from efficiently recombined *Kdm6b*-KO^{MX1} HSCs (Figure 4f). Two-weeks post-pIpC, there was already significant depletion of *Kdm6b*-KO^{MX1} HSCs (Figure 4g). But of the residual *Kdm6b*-KO^{MX1} HSCs, ~90% did show recombination of both *Kdm6b* alleles (Figure 4h). This indicates that pIpC-driven recombination of *Kdm6b* flox alleles using Mx1-CRE is efficient, but those HSCs differentiate rapidly under inflammatory stress and become depleted from the HSC pool.

Kdm6b-deficient HSCs are primed for differentiation

To examine the role of *Kdm6b* in HSC function in response to other proliferative stress, mice were injected with 5-FU. 5-FU is a myeloablative agent that kills cycling hematopoietic cells, forcing the quiescent HSCs into cycle to repopulate the depleted bone marrow⁴⁵. While *Kdm6b*-deficient mice were capable of initial hematopoietic recovery (Figure 5a), upon serial 5-FU injection both *Kdm6b*-Het^{VAV} and *Kdm6b*-KO^{VAV} mice showed significantly decreased survival (Figure 5b), indicative of impaired HSC regenerative capacity.

To examine the inflammatory response of *Kdm6b*-deficient HSCs without the confounding effects of Mx1-CRE, hematopoietic chimeras were generated by transplanting mice with 2.5×10^5 WBM from Control^{VAV}, *Kdm6b*-Het^{VAV} and *Kdm6b*-KO^{VAV} donors along with 2.5×10^5 wild-type WBM competitor cells and treated with pIpC or PBS (control) five-weeks post-transplant. *Kdm6b*-KO^{VAV} engraftment increased significantly in pIpC-treated recipients (Figure 5c), suggesting these HSCs differentiate more rapidly in response to inflammation. To investigate the acute kinetics of HSC response to inflammatory stress, mice were treated with two doses of pIpC and analyzed 24-hours after the second injection. While Control^{VAV} HSCs (Lineage- c-Kit+ EPCR+ CD48- CD150+; Sca-1 is excluded because it is IFN-responsive) increased post-pIpC, *Kdm6b*-Het^{VAV} and *Kdm6b*-KO^{VAV} HSCs showed no change (Figure 5d). But the total *Kdm6b*-KO^{VAV} progenitor cell pool (Lineage- c-Kit+ EPCR+; Figure 5d) expanded after pIpC. The changes in HSC and progenitor cell frequency between the genotypes could not be attributed to altered apoptotic response to pIpC (Figure 5e). Cell cycle analysis showed reduced quiescence amongst all HSC and progenitor genotypes following pIpC (Figure 5f). This indicates that upon

inflammatory stress, *Kdm6b*-KO^{VAV} HSCs differentiate to downstream progenitors, but fail to self-renew. Cumulatively, these data suggest that *Kdm6b* acts to limit the differentiation response of HSCs after inflammatory stress to preserve the HSC pool.

Kdm6b regulates the HSC stress response through the AP-1 transcription factor complex

Downregulation of the AP-1 transcription factor complex downregulation is associated with differentiation arrest^{47–49}. The AP-1 complex subunits *Fos* and *Jun* were over-expressed in *Kdm6b*-KO^{VAV} HSCs at basal conditions and upon inflammatory or myeloablative stress, *Fos* and *Jun* became even more over-expressed in *Kdm6b*-KO^{VAV} HSCs (Figure 6a,b), as did AP-1 target IER genes (*Dusp1*, *Zfp36*, and *Ier2*; Supplementary Figure 5). If downregulation of AP-1 inhibits differentiation, we hypothesized that AP-1 over-expression may enforce stem cell differentiation and drive depletion of *Kdm6b*-KO^{VAV} HSCs following proliferative stress. As such, ectopic expression of *Fos* and *Jun* in wild-type HSCs may produce a phenotype similar to *Kdm6b*-KO^{VAV} HSCs. Control^{VAV} c-Kit enriched WBM was co-transduced (Supplementary Figure 6a) with lentiviruses expressing either *Fos*-GFP or *Jun*-mCherry in parallel with empty vector control viruses and transplanted. Total donor-derived (CD45.2+) engraftment in both the control and over-expression recipients was comparable (Figure 6c). However, in the AP-1 over-expression recipients, there was a significant depletion of *Fos*-GFP and *Jun*-mCherry expressing cells in the blood (Figure 6d). By eight-weeks post-transplant, 90% of donor-derived cells were double negative (not expressing either *Fos* or *Jun*), despite representing only <25% of the initial transplanted population. BM analysis showed a significant reduction in AP-1 over-expressing progenitors (Figure 6e), which phenocopies loss of *Kdm6b* and implies upregulation of AP-1 forces HSC differentiation.

To determine if inhibiting *Fos* and *Jun* could rescue *Kdm6b*-KO^{VAV} HSC function, shRNAs were generated (Supplementary Figure 6b) and c-Kit enriched WBM from Control^{VAV} and *Kdm6b*-KO^{VAV} mice was transduced with LacZ (control) or *Fos*- (marked by GFP) / *Jun*- (marked by mCherry) targeting shRNA viruses (Supplementary Figure 6c) and transplanted into lethally irradiated mice. Knockdown of *Fos* and *Jun* significantly increased engraftment of *Kdm6b*-KO^{VAV} cells over all groups (Figure 6f), implying *Kdm6b*-deficient progenitor cells are extremely sensitive to modulation of AP-1 activity. There was no difference in peripheral blood engraftment between LacZ and *Fos*- / *Jun*-shRNA transduced Control^{VAV} cells, and there was equal transduction representation across all groups in donor-derived blood cells at 16-weeks post-transplant (Figure 6g). *Fos*- / *Jun*-knockdown also restored bone marrow progenitors in *Kdm6b*-KO^{VAV} recipients (Figure 6h) without biases in shRNA representation (Figure 6i). Thus, inhibiting AP-1 in *Kdm6b*-KO^{VAV} HSCs rescues their engraftment defects.

Kdm6b is required for self-renewal of MLL-AF9 leukemia-initiating cells

Over-expression of KDM6B can inhibit growth of M2/M3 AML cells, but has not M5 (granulocytic subtype) AML²². But as expression level does not always equate with activity, to clarify a function of *Kdm6b* in M5 AML, c-Kit enriched WBM from Control^{VAV}, *Kdm6b*-Het^{VAV} and *Kdm6b*-KO^{VAV} mice was transduced with the MLL-AF9 oncogene⁵⁰ and transplanted. Transduction efficiency and frequency of MLL-AF9+ GMPs (the

leukemia-initiating cells in this model) were comparable between genotypes (Supplementary Figure 7a). Four-weeks post-transplant there was a significant reduction in MLL-AF9 GFP+ cells in the blood in both *Kdm6b*-Het^{VAV} and *Kdm6b*-KO^{VAV} recipients (Supplementary Figure 7b). This correlated with increased survival (Figure 7a). There was no difference in spleen weights of moribund mice (Supplementary Figure 7c), but decreased leukemic GMPs in the bone marrow of *Kdm6b*-Het^{VAV} and *Kdm6b*-KO^{VAV} recipients (Figure 7b,c; Supplementary Figure 7d). Secondary transplant was performed with limiting doses of WBM from primary tumors to determine frequency of functional leukemia-initiating cells. Recipient mice were scored as positive if they developed AML (Figure 7d). *Kdm6b*-Het^{VAV} and *Kdm6b*-KO^{VAV} tumors had a three-fold reduction in leukemia-initiating cell frequency (Figure 7e).

To determine if *Kdm6b* is necessary for maintenance of MLL-AF9 AML, *Kdm6b*^{fl/fl} mice were crossed to ERT2-CRE mice²⁸. Post-tamoxifen analysis of *Kdm6b*-Het^{ERT2} mice showed complete floxing in HSCs (Supplementary Figure 7e), and there was no leaky CRE activity (Supplementary Figure 7f). c-Kit+ WBM was transduced with MLL-AF9 and transplanted. Recipients were treated with tamoxifen when the blood comprised ~10% GFP+ cells (Figure 7f). Of the mice surviving two-days after the last dose, GFP+ cells were reduced in *Kdm6b*-KO^{ERT2} recipients (Figure 7g). Either heterozygous or homozygous deletion of *Kdm6b* in pre-existing AML significantly extended survival (Figure 7h). GFP+ blasts two-days post-tamoxifen showed intact floxed alleles in both *Kdm6b*-HET^{ERT2} and *Kdm6b*-KO^{ERT2} cells (Supplementary Figure 7g). Analysis of moribund animals showed many mice succumbed to AML with intact floxed alleles (Supplementary Figure 7h), indicating a strong pressure to maintain *Kdm6b*. *Fos* and *Jun* were also over-expressed in *Kdm6b*-deficient MLL-AF9 cells (Supplemental Figure 7i).

As we observed gene expression changes in *Kdm6b*-KO^{VAV} HSCs occurred without significant chromatin alterations, to determine if the role of Kdm6b in MLL-AF9 AML was also demethylase-independent, primary AML cells were cultured in GSK-J4, a small molecule that inhibits the demethylase domain of Kdm6b (and also Utx1)⁹. The dose response to GSK-J4 was identical between genotype (Figure 7i), indicating that inhibition Kdm6b demethylase activity has no effect MLL-AF9 AML. To examine this *in vivo*, primary *Kdm6b*-KO^{VAV} MLL-AF9 AMLs were transduced with lentiviruses expressing either full-length *Kdm6b* or a catalytically-dead Kdm6b point mutant (*Kdm6b*^{H1388A})^{6, 51}. While expression of full-length *Kdm6b* restored leukemic potential, so did *Kdm6b*^{H1388A} (Figure 7j). Cumulatively, these data suggest the functions of Kdm6b in normal and malignant stem cells are largely H3K27me3-independent.

Kdm6b supports context-dependent leukemogenesis

To investigate *Kdm6b* in other leukemias, c-Kit+ WBM was transduced with a retrovirus expressing Notch1 Intra-Cellular Domain (NICD), a model that recapitulates human T-ALL⁵². 1.0×10^5 cells were transplanted (Figure 8a) with similar transduction efficiencies (Figure 8b). Four-weeks post-transplant, NICD-GFP+ cells were increased in the blood of *Kdm6b*-KO^{VAV} recipients (Figure 8c). But despite this, and unlike MLL-AF9 AML, loss of *Kdm6b* did not produce a survival benefit in adult T-ALL (Figure 8d). Because these results

were disparate with a previous NICD study using fetal liver-derived *Kdm6b*-deficient cells²¹, c-Kit⁺ cells from E14.5 fetal liver were transduced with NICD and transplanted (Figure 8e). Four-weeks post-transplant showed equivalent NICD-GFP⁺ in recipient blood (Figure 8f). However, *Kdm6b*-Het^{VAV} and *Kdm6b*-KO^{VAV} recipients showed a significant survival benefit (Figure 8g), and mice alive after 100-days showed a complete dearth of T-ALL cells (data not shown) despite being initially engrafted. This implies a unique requirement for *Kdm6b* in sustaining T-ALL cells of fetal origin. This result was reversed in fetal-derived MLL-AF9 AML (Figure 8h–j) where no survival benefit was observed in a *Kdm6b*-deficient background. The differences between fetal- versus adult-derived leukemias could not be explained by variation in fetal HSC content (Figure 8k,l).

DISCUSSION

We show loss of *Kdm6b* compromises self-renewal of both normal and leukemic stem cells (dependent on lineage subtype and developmental stage). Our results suggest *KDM6B* mutations are not observed in hematopoietic malignancies (or clonal hematopoiesis) as this would result in loss of that clone due to competitive disadvantage. This was observed experimentally when *Kdm6b* was deleted after the initiation of MLL-AF9 AML and the “wild-type” blasts outcompeted those that lost *Kdm6b*.

We show the major functions of *Kdm6b* in HSCs appear unrelated to chromatin regulation, but rather demethylase-independent regulation of stress response gene expression programs. As chromatin architecture in *Kdm6b*-KO^{Vav} HSCs is largely unaltered, the gene expression differences may be secondary effects downstream of master regulators like AP-1. Upon proliferative stress, *Kdm6b*-deficient HSCs differentiate rapidly and self-renew inefficiently, due at least in part to upregulation of *Fos* and *Jun*. Over-expression of AP-1 in wild-type progenitors phenocopied loss of *Kdm6b*, and reducing their expression in *Kdm6b*-deficient HSCs restored engraftment potential. Enforced expression of *Fos* in M1 leukemia cells mimics what was observed here, with increased differentiation and reduced disease aggressiveness⁵³. Moreover, prolonged expression of *Fos* in transgenic mouse HSCs decreases functional potential⁵⁴. This implicates *Fos* over-expression as a major determinant of the *Kdm6b*-deficient HSC phenotype. Indeed, the *Fos* locus was one of the only genomic regions that showed a difference in chromatin accessibility in *Kdm6b*-KO^{Vav} HSCs. But the mechanisms through which AP-1 and *Kdm6b* interact in HSCs and regulate each other and their target genes remains unclear. Given improving genomic technologies in regards to low cell inputs, it is possible this can be directly tested in the future.

Our data suggest the potential of *KDM6B* as a therapeutic target for leukemia depends on developmental and cellular context. GSK-J4, which binds to the catalytic domain and inhibits demethylase activity of both *KDM6B* and *UTX1*⁹, has been cited as a potential clinical agent in blood cancers^{21, 55}. It is possible the activity observed in other studies occurs primarily through *UTX1* inhibition, which is a potent hematopoietic tumor suppressor⁵⁶. Our data suggest inhibiting demethylase activity of *KDM6B* would likely be ineffective, and that more specific effects could be achieved by targeting the domains that regulate its unique functions in HSCs. Nevertheless, *KDM6B* may still represent an attractive therapeutic target in certain contexts as haploinsufficiency had modest effects for

normal HSCs, but both heterozygous and homozygous loss of *Kdm6b* impeded adult-derived MLL-AF9 AML with similar kinetics. Thus, a 50% inhibition could be deleterious for leukemia-initiating cells, without being toxic to normal HSCs. Cumulatively, our data show that *Kdm6b* is necessary for HSC maintenance in response to proliferative stress, and present KDM6B as a potential therapeutic target in leukemias depending on the subtype and developmental context.

Supplementary Material

Refer to Web version on PubMed Central for supplementary material.

ACKNOWLEDGEMENTS

We thank and Dr. Martin Matzuk (Baylor College of Medicine) for providing *Kdm6b*^{fl/fl} mice, Dr. Lukas Wartman (Washington University) for providing *Utx*^{fl/fl} mice, and Dr. Jeff Magee (Washington University) for providing MLL-AF9 retroviral plasmid. We thank the Alvin J. Siteman Cancer Center at Washington University for use of the Siteman Flow Cytometry Core, supported in part by NCI Grant CA91842. We thank the Genome Technology Access Center at Washington University for genomic analysis, partially supported by NCI Grant CA91842 and by ICTS/CTSA Grant UL1TR000448 NIH.

This work was supported by the National Institutes of Health (R01DK102428), the Edward Mallinckrodt Jr. Foundation, the American Society of Hematology, the V Foundation, Gabrielle's Angel Foundation, and the Sidney Kimmel Foundation (all to G.A.C.). Bioinformatics analysis was supported by the Washington University Center for Regenerative Medicine. C.M. was supported by NIH T32HL007088, and NIH DK111058-01. E.L.O. was supported by NIH 5T32CA113275-10 and NIH F31DK114951. H.C. was supported by a post-doctoral scholar award from the American Society of Hematology and an Edward P. Evans Foundation Young Investigator Award. G.A.C. is a Leukemia and Lymphoma Society scholar.

REFERENCES

- Hong S, Cho YW, Yu LR, Yu H, Veenstra TD, Ge K. Identification of JmjC domain-containing UTX and JMJD3 as histone H3 lysine 27 demethylases. *Proc Natl Acad Sci U S A* 2007;104(47):18439–44. [PubMed: 18003914]
- Bannister AJ, Kouzarides T. Regulation of chromatin by histone modifications. *Cell Res* 2011;21(3):381–95. [PubMed: 21321607]
- Lan F, Bayliss PE, Rinn JL, Whetstine JR, Wang JK, Chen S, et al. A histone H3 lysine 27 demethylase regulates animal posterior development. *Nature* 2007;449(7163):689–94. [PubMed: 17851529]
- Sen GL, Webster DE, Barragan DI, Chang HY, Khavari PA. Control of differentiation in a self-renewing mammalian tissue by the histone demethylase JMJD3. *Genes Dev* 2008;22(14):1865–70. [PubMed: 18628393]
- Burgold T, Voituron N, Caganova M, Tripathi PP, Menuet C, Tusi BK, et al. The H3K27 demethylase JMJD3 is required for maintenance of the embryonic respiratory neuronal network, neonatal breathing, and survival. *Cell Rep* 2012;2(5):1244–58. [PubMed: 23103168]
- Agger K, Cloos PA, Christensen J, Pasini D, Rose S, Rappsilber J, et al. UTX and JMJD3 are histone H3K27 demethylases involved in HOX gene regulation and development. *Nature* 2007;449(7163):731–4. [PubMed: 17713478]
- De Santa F, Narang V, Yap ZH, Tusi BK, Burgold T, Austenaa L, et al. Jmjd3 contributes to the control of gene expression in LPS-activated macrophages. *Embo J* 2009;28(21):3341–52. [PubMed: 19779457]
- De Santa F, Totaro MG, Prosperini E, Notarbartolo S, Testa G, Natoli G. The histone H3 lysine-27 demethylase Jmjd3 links inflammation to inhibition of polycomb-mediated gene silencing. *Cell* 2007;130(6):1083–94. [PubMed: 17825402]

9. Kruidenier L, Chung CW, Cheng Z, Liddle J, Che K, Joberty G, et al. A selective jumonji H3K27 demethylase inhibitor modulates the proinflammatory macrophage response. *Nature* 2012;488(7411):404–8. [PubMed: 22842901]
10. Wijayatunge R, Chen LF, Cha YM, Zannas AS, Frank CL, West AE. The histone lysine demethylase Kdm6b is required for activity-dependent preconditioning of hippocampal neuronal survival. *Mol Cell Neurosci* 2014;61:187–200. [PubMed: 24983519]
11. Agger K, Cloos PA, Rudkjaer L, Williams K, Andersen G, Christensen J, et al. The H3K27me3 demethylase JMJD3 contributes to the activation of the INK4A-ARF locus in response to oncogene- and stress-induced senescence. *Genes Dev* 2009;23(10):1171–6. [PubMed: 19451217]
12. Barradas M, Anderton E, Acosta JC, Li S, Banito A, Rodriguez-Niedenfuhr M, et al. Histone demethylase JMJD3 contributes to epigenetic control of INK4a/ARF by oncogenic RAS. *Genes Dev* 2009;23(10):1177–82. [PubMed: 19451218]
13. Ohguchi H, Harada T, Sagawa M, Kikuchi S, Tai YT, Richardson PG, et al. KDM6B modulates MAPK pathway mediating multiple myeloma cell growth and survival. *Leukemia* 2017;31(12):2661–9. [PubMed: 28487543]
14. Greenblatt SM, Nimer SD. Chromatin modifiers and the promise of epigenetic therapy in acute leukemia. *Leukemia* 2014;28(7):1396–406. [PubMed: 24609046]
15. Abdel-Wahab O, Levine RL. Mutations in epigenetic modifiers in the pathogenesis and therapy of acute myeloid leukemia. *Blood* 2013;121(18):3563–72. [PubMed: 23640996]
16. Cancer Genome Atlas Research N. Genomic and epigenomic landscapes of adult de novo acute myeloid leukemia. *N Engl J Med* 2013;368(22):2059–74. [PubMed: 23634996]
17. Mar BG, Bullinger L, Basu E, Schlis K, Silverman LB, Dohner K, et al. Sequencing histone-modifying enzymes identifies UTX mutations in acute lymphoblastic leukemia. *Leukemia* 2012;26(8):1881–3. [PubMed: 22377896]
18. Kiel MJ, Sahasrabudhe AA, Rolland DC, Velusamy T, Chung F, Schaller M, et al. Genomic analyses reveal recurrent mutations in epigenetic modifiers and the JAK-STAT pathway in Sezary syndrome. *Nat Commun* 2015;6:8470. [PubMed: 26415585]
19. Wei Y, Chen R, Dimicoli S, Bueso-Ramos C, Neuberg D, Pierce S, et al. Global H3K4me3 genome mapping reveals alterations of innate immunity signaling and overexpression of JMJD3 in human myelodysplastic syndrome CD34+ cells. *Leukemia* 2013;27(11):2177–86. [PubMed: 23538751]
20. Anderton JA, Bose S, Vockerodt M, Vrzalikova K, Wei W, Kuo M, et al. The H3K27me3 demethylase, KDM6B, is induced by Epstein-Barr virus and over-expressed in Hodgkin’s Lymphoma. *Oncogene* 2011;30(17):2037–43. [PubMed: 21242977]
21. Ntziachristos P, Tsigiris A, Welstead GG, Trimarchi T, Bakogianni S, Xu L, et al. Contrasting roles of histone 3 lysine 27 demethylases in acute lymphoblastic leukaemia. *Nature* 2014.
22. Yu SH, Zhu KY, Chen J, Liu XZ, Xu PF, Zhang W, et al. JMJD3 facilitates C/EBPβ-centered transcriptional program to exert oncorepressor activity in AML. *Nat Commun* 2018;9(1):3369. [PubMed: 30135572]
23. Wei Y, Zheng H, Bao N, Jiang S, Bueso-Ramos CE, Khoury J, et al. KDM6B overexpression activates innate immune signaling and impairs hematopoiesis in mice. *Blood Adv* 2018;2(19):2491–504. [PubMed: 30275007]
24. Iwamori N, Iwamori T, Matzuk MM. H3K27 demethylase, JMJD3, regulates fragmentation of spermatogonial cysts. *PLoS ONE* 2013;8(8):e72689. [PubMed: 23967333]
25. Wang C, Lee JE, Cho YW, Xiao Y, Jin Q, Liu C, et al. UTX regulates mesoderm differentiation of embryonic stem cells independent of H3K27 demethylase activity. *Proc Natl Acad Sci U S A* 2012;109(38):15324–9. [PubMed: 22949634]
26. Georgiades P, Ogilvy S, Duval H, Licence DR, Charnock-Jones DS, Smith SK, et al. VavCre transgenic mice: a tool for mutagenesis in hematopoietic and endothelial lineages. *Genesis* 2002;34(4):251–6. [PubMed: 12434335]
27. Kuhn R, Schwenk F, Aguet M, Rajewsky K. Inducible Gene Targeting in Mice. *Science* 1995;269(5229):1427–9. [PubMed: 7660125]
28. Hayashi S, McMahon AP. Efficient recombination in diverse tissues by a tamoxifen-inducible form of Cre: a tool for temporally regulated gene activation/inactivation in the mouse. *Dev Biol* 2002;244(2):305–18. [PubMed: 11944939]

29. Dobin A, Davis CA, Schlesinger F, Drenkow J, Zaleski C, Jha S, et al. STAR: ultrafast universal RNA-seq aligner. *Bioinformatics* 2013;29(1):15–21. [PubMed: 23104886]
30. Liao Y, Smyth GK, Shi W. featureCounts: an efficient general purpose program for assigning sequence reads to genomic features. *Bioinformatics* 2014;30(7):923–30. [PubMed: 24227677]
31. Liao Y, Smyth GK, Shi W. The Subread aligner: fast, accurate and scalable read mapping by seed-and-vote. *Nucleic Acids Res* 2013;41(10):e108. [PubMed: 23558742]
32. Patro R, Mount SM, Kingsford C. Sailfish enables alignment-free isoform quantification from RNA-seq reads using lightweight algorithms. *Nat Biotechnol* 2014;32(5):462–4. [PubMed: 24752080]
33. Subramanian A, Tamayo P, Mootha VK, Mukherjee S, Ebert BL, Gillette MA, et al. Gene set enrichment analysis: a knowledge-based approach for interpreting genome-wide expression profiles. *Proc Natl Acad Sci U S A* 2005;102(43):15545–50. [PubMed: 16199517]
34. Schmidl C, Rendeiro AF, Sheffield NC, Bock C. ChIPmentation: fast, robust, low-input ChIP-seq for histones and transcription factors. *Nat Methods* 2015;12(10):963–5. [PubMed: 26280331]
35. Langmead B, Salzberg SL. Fast gapped-read alignment with Bowtie 2. *Nat Methods* 2012;9(4):357–9. [PubMed: 22388286]
36. Starmer J, Magnuson T. Detecting broad domains and narrow peaks in ChIP-seq data with hiddenDomains. *BMC Bioinformatics* 2016;17:144. [PubMed: 27009150]
37. Carroll TS, Liang Z, Salama R, Stark R, de Santiago I. Impact of artifact removal on ChIP quality metrics in ChIP-seq and ChIP-exo data. *Front Genet* 2014;5:75. [PubMed: 24782889]
38. Ramirez F, Ryan DP, Gruning B, Bhardwaj V, Kilpert F, Richter AS, et al. deepTools2: a next generation web server for deep-sequencing data analysis. *Nucleic Acids Res* 2016;44(W1):W160–5. [PubMed: 27079975]
39. Neph S, Kuehn MS, Reynolds AP, Haugen E, Thurman RE, Johnson AK, et al. BEDOPS: high-performance genomic feature operations. *Bioinformatics* 2012;28(14):1919–20. [PubMed: 22576172]
40. Corces MR, Trevino AE, Hamilton EG, Greenside PG, Sinnott-Armstrong NA, Vesuna S, et al. An improved ATAC-seq protocol reduces background and enables interrogation of frozen tissues. *Nat Methods* 2017;14(10):959–62. [PubMed: 28846090]
41. Li Q, Zou J, Wang M, Ding X, Chepelev I, Zhou X, et al. Critical role of histone demethylase Jmjd3 in the regulation of CD4+ T-cell differentiation. *Nat Commun* 2014;5:5780. [PubMed: 25531312]
42. Hu Y, Smyth GK. ELDA: extreme limiting dilution analysis for comparing depleted and enriched populations in stem cell and other assays. *J Immunol Methods* 2009;347(1–2):70–8. [PubMed: 19567251]
43. Kirschner K, Chandra T, Kiselev V, Flores-Santa Cruz D, Macaulay IC, Park HJ, et al. Proliferation Drives Aging-Related Functional Decline in a Subpopulation of the Hematopoietic Stem Cell Compartment. *Cell Rep* 2017;19(8):1503–11. [PubMed: 28538171]
44. Tullai JW, Schaffer ME, Mullenbrock S, Sholder G, Kasif S, Cooper GM. Immediate-early and delayed primary response genes are distinct in function and genomic architecture. *J Biol Chem* 2007;282(33):23981–95. [PubMed: 17575275]
45. Venezia TA, Merchant AA, Ramos CA, Whitehouse NL, Young AS, Shaw CA, et al. Molecular signatures of proliferation and quiescence in hematopoietic stem cells. *PLoS Biol* 2004;2(10):e301. [PubMed: 15459755]
46. Fortier ME, Kent S, Ashdown H, Poole S, Boksa P, Luheshi GN. The viral mimic, polyinosinic:polycytidylic acid, induces fever in rats via an interleukin-1-dependent mechanism. *Am J Physiol Regul Integr Comp Physiol* 2004;287(4):R759–66. [PubMed: 15205185]
47. Yamazaki S, Tanaka Y, Araki H, Kohda A, Sanematsu F, Arasaki T, et al. The AP-1 transcription factor JunB is required for Th17 cell differentiation. *Sci Rep* 2017;7(1):17402. [PubMed: 29234109]
48. Leppa S, Eriksson M, Saffrich R, Ansorge W, Bohmann D. Complex functions of AP-1 transcription factors in differentiation and survival of PC12 cells. *Mol Cell Biol* 2001;21(13):4369–78. [PubMed: 11390664]

49. Han B, Rorke EA, Adhikary G, Chew YC, Xu W, Eckert RL. Suppression of AP1 transcription factor function in keratinocyte suppresses differentiation. *PLoS One* 2012;7(5):e36941. [PubMed: 22649503]
50. Krivtsov AV, Twomey D, Feng Z, Stubbs MC, Wang Y, Faber J, et al. Transformation from committed progenitor to leukaemia stem cell initiated by MLL-AF9. *Nature* 2006;442(7104):818–22. [PubMed: 16862118]
51. Xiang Y, Zhu Z, Han G, Lin H, Xu L, Chen CD. JMJD3 is a histone H3K27 demethylase. *Cell Res* 2007;17(10):850–7. [PubMed: 17923864]
52. Pear WS, Aster JC, Scott ML, Hasserjian RP, Soffer B, Sklar J, et al. Exclusive development of T cell neoplasms in mice transplanted with bone marrow expressing activated Notch alleles. *J Exp Med* 1996;183(5):2283–91. [PubMed: 8642337]
53. Lord KA, Abdollahi A, Hoffman-Liebermann B, Liebermann DA. Proto-oncogenes of the fos/jun family of transcription factors are positive regulators of myeloid differentiation. *Mol Cell Biol* 1993;13(2):841–51. [PubMed: 8423806]
54. Okada S, Fukuda T, Inada K, Tokuhisa T. Prolonged expression of c-fos suppresses cell cycle entry of dormant hematopoietic stem cells. *Blood* 1999;93(3):816–25. [PubMed: 9920830]
55. Li Y, Zhang M, Sheng M, Zhang P, Chen Z, Xing W, et al. Therapeutic potential of GSK-J4, a histone demethylase KDM6B/JMJD3 inhibitor, for acute myeloid leukemia. *J Cancer Res Clin Oncol* 2018;144(6):1065–77. [PubMed: 29594337]
56. Van der Meulen J, Sanghvi V, Mavrikis K, Durinck K, Fang F, Matthijssens F, et al. The H3K27me3 demethylase UTX is a gender-specific tumor suppressor in T-cell acute lymphoblastic leukemia. *Blood* 2015;125(1):13–21. [PubMed: 25320243]

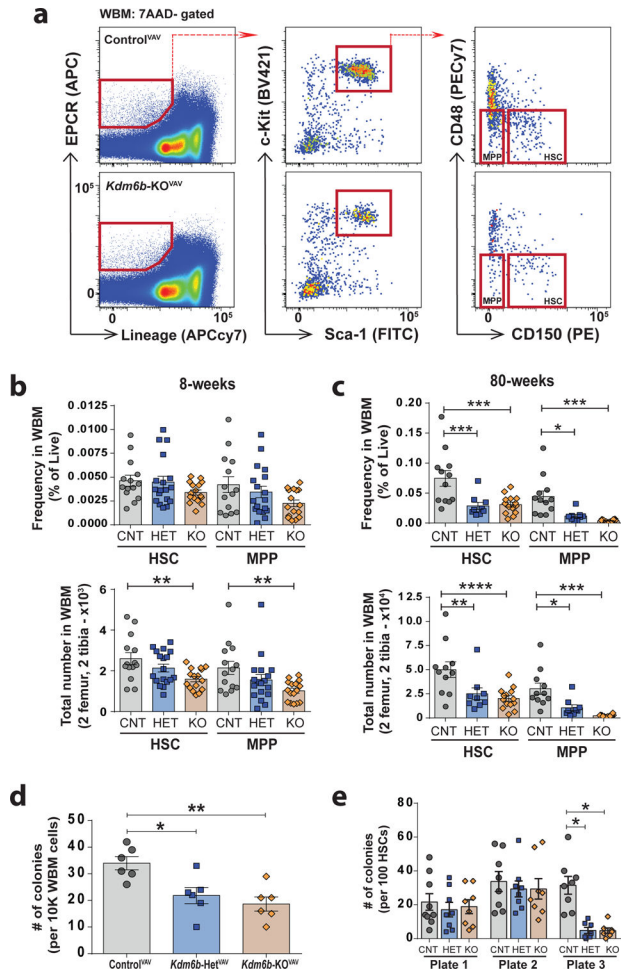


Figure 1: Loss of *Kdm6b* results in depletion of primitive hematopoietic progenitors. (a) Flow cytometry gating scheme to identify hematopoietic stem cells (HSCs) and multipotent progenitors (MPPs) in bone marrow (BM) of eight-week old Control^{VAV} (top) or *Kdm6b*-KO^{VAV} mice (bottom). (b) Frequency and absolute number of HSCs and MPPs in BM of eight-week old Control^{VAV} (CNT, *n*=14), *Kdm6b*-Het^{VAV} (HET, *n*=18), and *Kdm6b*-KO^{VAV} (KO, *n*=16) mice. (c) Frequency and absolute number of HSCs and MPPs in BM of 80-week old Control^{VAV} (CNT, *n*=12), *Kdm6b*-Het^{VAV} (HET, *n*=9), and *Kdm6b*-KO^{VAV} (KO, *n*=14) mice. (d) Colony-forming units per 1×10⁴ BM cells from young Control^{VAV} (*n*=6), *Kdm6b*-Het^{VAV} (*n*=6) and *Kdm6b*-KO^{VAV} (*n*=6) mice. (e) Colonies generated in Methocult serial replating. For plate 1, 100 HSCs were sorted from individual young mice (*n*=5–9), then 1×10⁴ cells were plated for serial rounds. **p*<0.05, ***p*<0.01, ****p*<0.001, *****p*<0.0001. Mean ± S.E.M. values are shown.

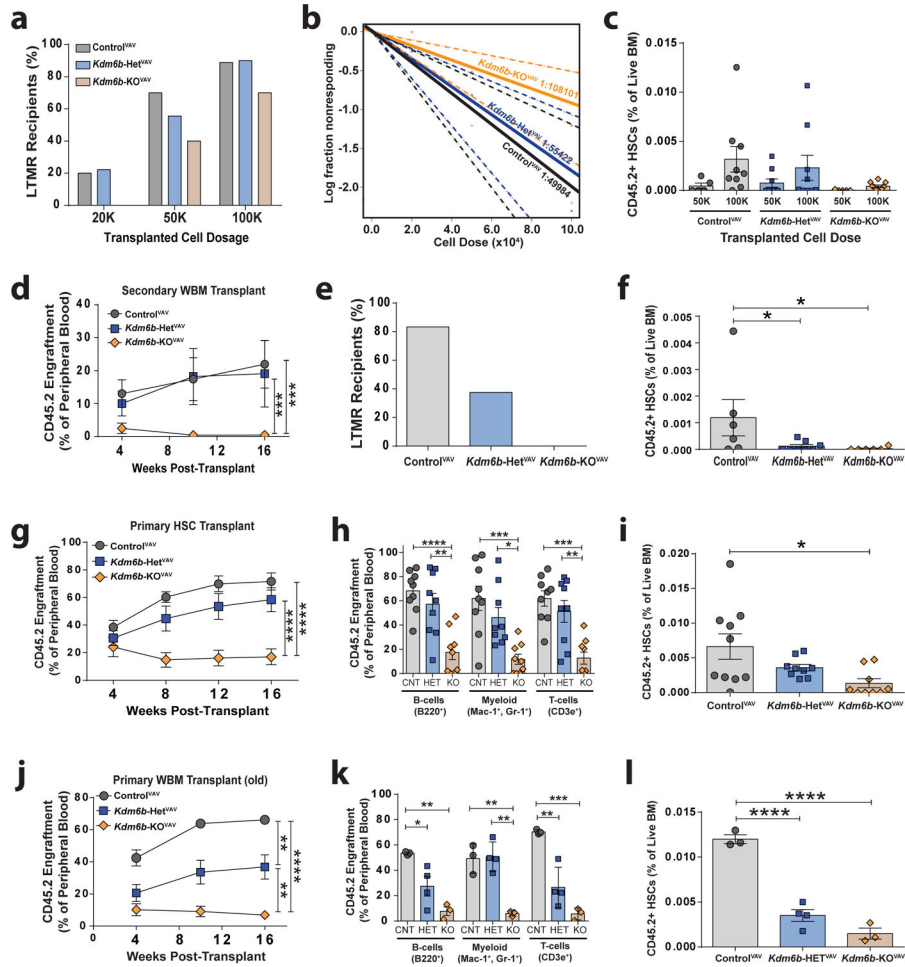


Figure 2: *Kdm6b* is required for HSC self-renewal.

(a) Proportion of long-term multi-lineage reconstituted (LTMR) recipient mice at stated cell doses 16-weeks post-transplant ($n=9-10$ per genotype at each cell dose). (b) Frequency of long-term repopulating cells using a maximum likelihood estimate with extreme limiting dilution analysis (ELDA) software. (c) Frequency of donor-derived (CD45.2+) HSCs in BM of recipient mice 18-weeks post-transplant. (d) Peripheral blood engraftment in secondary transplants of 3.0×10^6 BM from LTMR primary recipient mice ($n=6-8$). (e) Proportion of LTMR secondary recipient mice transplanted with Control^{VAV} ($n=6$), *Kdm6b*-Het^{VAV} ($n=8$), and *Kdm6b*-KO^{VAV} ($n=6$) primary BM. (f) Frequency of donor-derived HSCs in BM of secondary recipient mice 18-weeks post-transplant. (g) Donor-derived peripheral blood engraftment from primary transplant of 200 HSCs from Control^{VAV} ($n=10$), *Kdm6b*-Het^{VAV} ($n=9$), and *Kdm6b*-KO^{VAV} ($n=9$) mice. (h) Donor-derived chimerism in blood lineages 16-weeks post-transplant of 200 HSCs. (i) Frequency of donor-derived HSCs in BM of recipient mice 18-weeks post-transplant of 200 HSCs. (j) Donor-derived peripheral blood engraftment from competitive transplant of BM from aged Control^{VAV} ($n=3$), *Kdm6b*-Het^{VAV} ($n=4$), and *Kdm6b*-KO^{VAV} ($n=3$) mice. (k) Donor-derived chimerism in blood lineages 16-weeks post-transplant of aged BM. (l) Frequency of donor-derived HSCs in recipient mice 18-weeks

post-transplant of aged BM. * $p < 0.05$, ** $p < 0.01$, *** $p < 0.001$, **** $p < 0.0001$. Mean \pm S.E.M. values are shown.

Author Manuscript

Author Manuscript

Author Manuscript

Author Manuscript

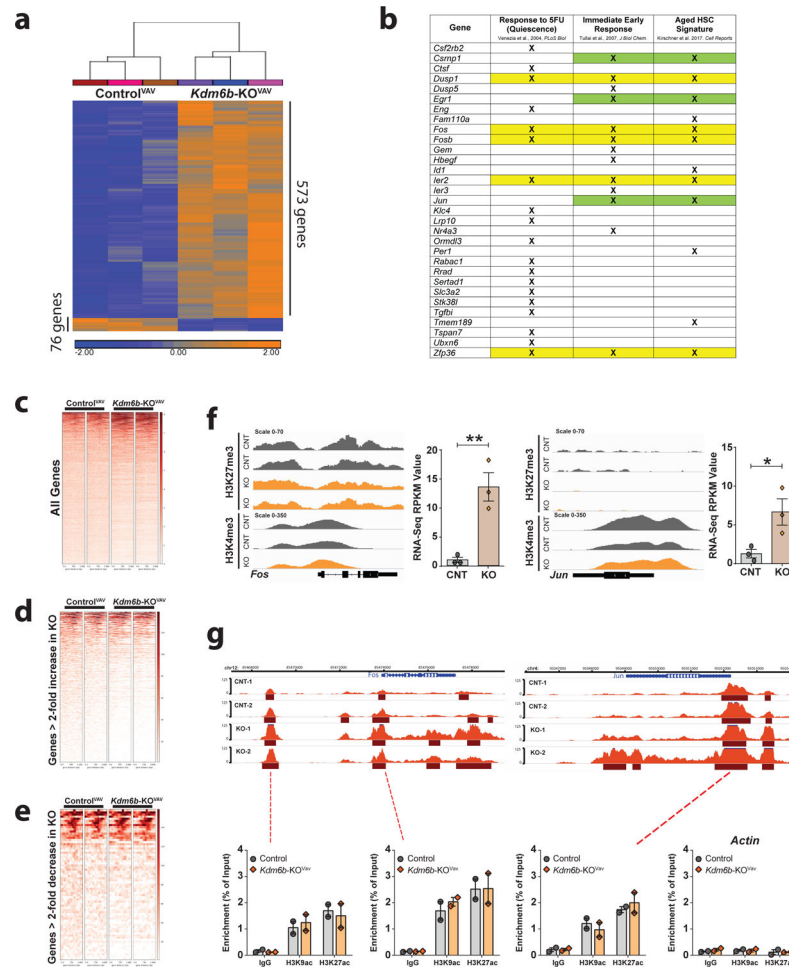


Figure 3: *Kdm6b* loss leads to a stress response gene expression signature in HSCs independent of chromatin changes.

(a) Hierarchical clustering of genes with >2-fold expression change (adjusted p -value < 0.05) in *Kdm6b*-KO^{VAV} HSCs compared to Control^{VAV} HSCs. (b) Overlap of genes upregulated in *Kdm6b*-KO^{VAV} HSCs which are downregulated in wild-type HSCs in response to 5-FU, immediate early response genes, and genes upregulated in aging HSCs. Yellow shading signifies genes identified in all comparisons. H3K27me3 distribution \pm 5Kb from transcriptional start sites (TSS) in all genes (c), for 573 genes with >2-fold increased expression in *Kdm6b*-KO^{VAV} HSCs (d), and for 76 genes with >2-fold decreased expression in *Kdm6b*-KO^{VAV} HSCs (e). (f) H3K27me3 and H3K4me3 profiles (left) and RNA-seq expression values (right) of *Fos* and *Jun* in Control^{VAV} HSCs and *Kdm6b*-KO^{VAV} HSCs. * p <0.05, ** p <0.01. Mean \pm S.E.M. values are shown. (g) ATAC-seq profiles of *Fos* and *Jun* in control (CNT) and *Kdm6b*-KO^{VAV} (KO) HSCs. Shown underneath is enrichment of other activating histone marks at relevant sites of open chromatin. *Actin* is shown as a negative control locus for ChIP-qPCR.

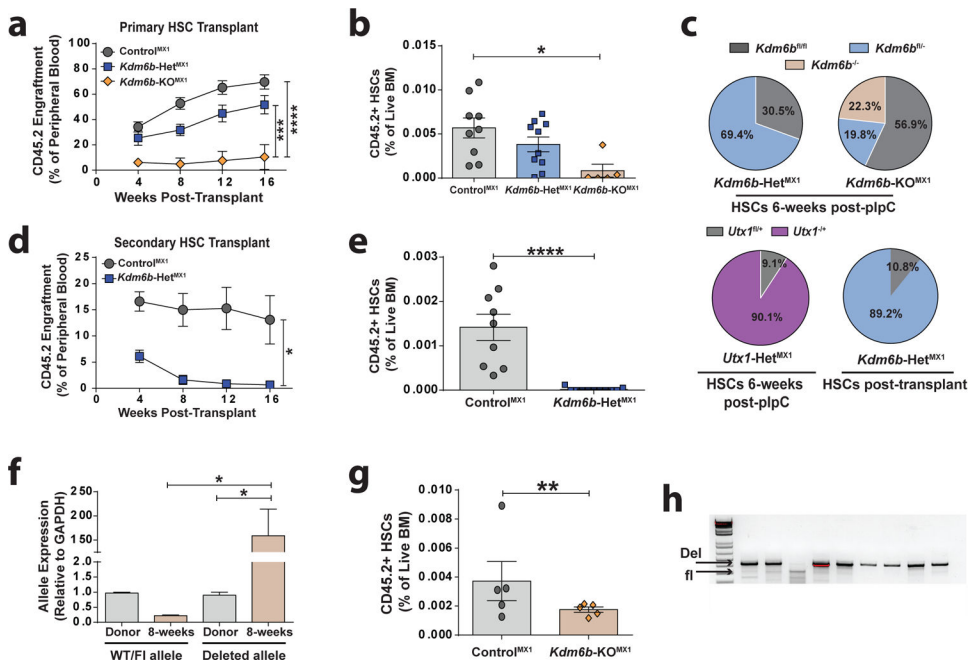


Figure 4: Inflammatory stress rapidly depletes *Kdm6b*-deficient HSCs.

(a) Peripheral blood engraftment of mice transplanted with 200 HSCs from Control^{MX1} ($n=9$), *Kdm6b*-HET^{MX1} ($n=10$), and *Kdm6b*-KO^{MX1} ($n=5$) mice. (b) Frequency of donor-derived HSCs in BM of primary recipient mice at 18-weeks post-transplant. (c) Efficiency of Mx1-CRE driven floxed allele recombination in HSCs from mice six-weeks post-pIpC treatment, as well as post-primary transplant in *Kdm6b*-HET^{MX1} HSCs. (d) Peripheral blood engraftment of secondary recipients transplanted with 200 Control^{MX1} ($n=9$) and *Kdm6b*-Het^{MX1} ($n=11$) HSCs from primary recipients. (e) Frequency of donor-derived HSCs in BM of secondary recipient mice 18-weeks post-transplant. (f) qPCR quantification of floxed:deleted *Kdm6b* allele ratio in *Kdm6b*-KO^{MX1} granulocytes pre- and post-pIpC treatment. (g) Donor-derived HSC frequency in the bone marrow of recipient mice two-weeks post-pIpC treatment. (h) Representative PCR analysis of genomic DNA from colonies derived from single HSCs showing floxed allele recombination efficiency in individual *Kdm6b*-KO^{MX1} HSCs two-weeks post-pIpC. * $p<0.05$, ** $p<0.01$, *** $p<0.001$, **** $p<0.0001$. Mean \pm S.E.M. values are shown.

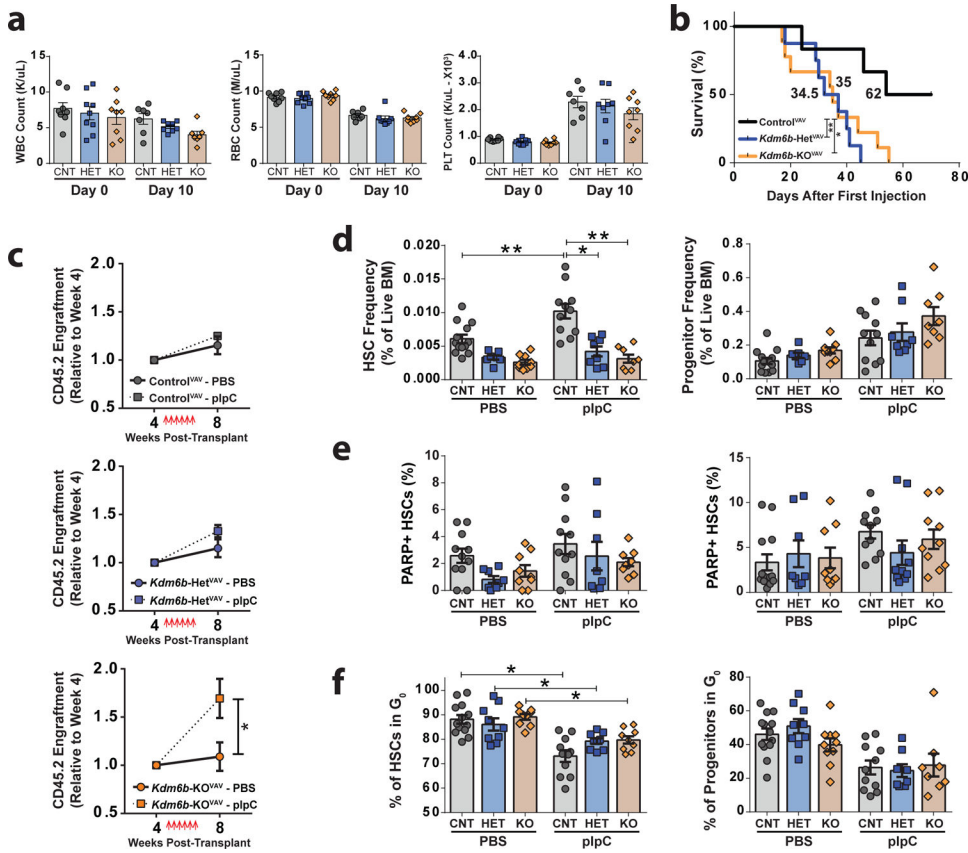


Figure 5: *Kdm6b*-deficient HSCs are primed for differentiation.

(a) Blood counts showing hematopoietic recovery of white blood cells (WBC), red blood cells (RBC) and platelets (PLT) in Control^{VAV} (CNT), *Kdm6b*-HET^{VAV} (HET) and *Kdm6b*-KO^{VAV} (KO) mice 10-days after injection with 5-FU ($n=6-9$). (b) Kaplan-Meier survival curve comparing time to morbidity of Control^{VAV} ($n=8$), *Kdm6b*-Het^{VAV} ($n=8$), and *Kdm6b*-KO^{VAV} ($n=8$) mice after serial 5-FU treatment (weekly injections). (c) Relative donor-derived peripheral-blood chimerism following treatment (red arrows) of hematopoietic chimeras with pIpC (dashed line) or PBS (control). (d) HSC and progenitor cell frequency 24-hours after two doses of PBS (control) or pIpC in Control^{VAV} (CNT), *Kdm6b*-HET^{VAV} (HET) and *Kdm6b*-KO^{VAV} (KO) mice ($n=6-16$). (e) Apoptosis analysis showing proportion of PARP+ HSCs and progenitors 24-hours after two doses of either PBS or pIpC. (f) Cell cycle analysis showing proportion of quiescent (G₀) HSCs and progenitors 24-hours after two doses of either PBS or pIpC. * $p<0.05$, ** $p<0.01$, *** $p<0.001$, **** $p<0.001$. Mean \pm S.E.M. values are shown.

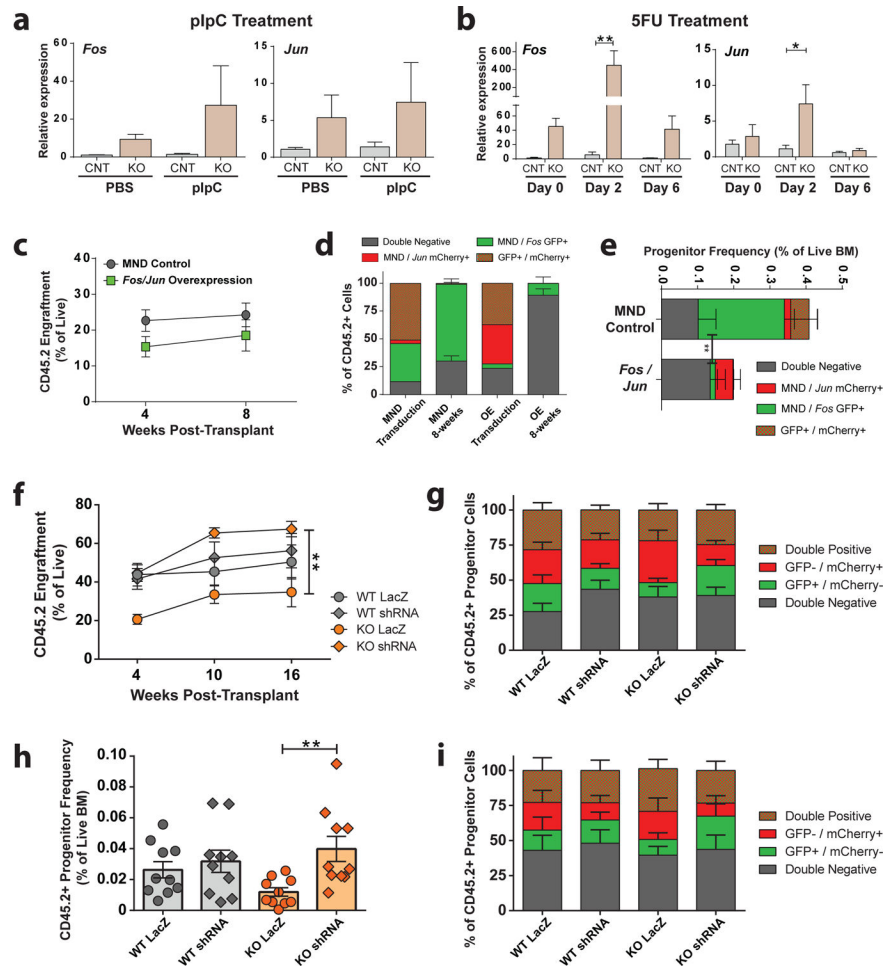


Figure 6: Kdm6b regulates the HSC stress response through the AP-1 transcription factor complex.

(a) Expression of AP-1 components *Jun* and *Fos* in Control^{VAV} and *Kdm6b*-KO^{VAV} HSCs after PBS (control) or two-doses of plpC ($n=3$). (b) Expression of *Jun* and *Fos* in Control^{VAV} and *Kdm6b*-KO^{VAV} HSCs during recovery from a single dose of 5-FU ($n=3-5$). (c) Donor-derived peripheral blood engraftment of wild-type BM progenitors transduced with pMND-*Fos*-GFP and pMND-*Jun*-mCherry, or respective empty vector control lentiviruses ($n=5$). (d) Proportion of donor-derived cells expressing each lentivirus combination in peripheral blood at eight-weeks post-transplant compared to initial transduction efficiency. (e) Proportion of donor-derived progenitor cells (Lineage- c-Kit+ Sca-1+) expressing each lentivirus combination in BM eight-weeks post-transplant. (f) Donor-derived peripheral blood engraftment of Control^{VAV} (WT) and *Kdm6b*-KO^{VAV} (KO) BM progenitor cells transduced with lentiviruses expressing shRNAs against *Fos* or *Jun* (shRNA), or respective *LacZ*-targeting lentiviruses ($n=10$). (g) Proportion of donor-derived cells expressing each lentivirus combination in peripheral blood at 16-weeks post-transplant. *LacZ* = *LacZ*-shRNA-mCherry / *LacZ*-shRNA-GFP; shRNA = *Jun*-shRNA-mCherry / *Fos*-shRNA-GFP. (h) Frequency of donor-derived progenitor cells in the BM of recipient mice 18-weeks post-transplant. (i) Proportion of donor-derived BM progenitor cells expressing each lentivirus combination. * $p<0.05$, ** $p<0.01$. Mean \pm S.E.M. values are shown.

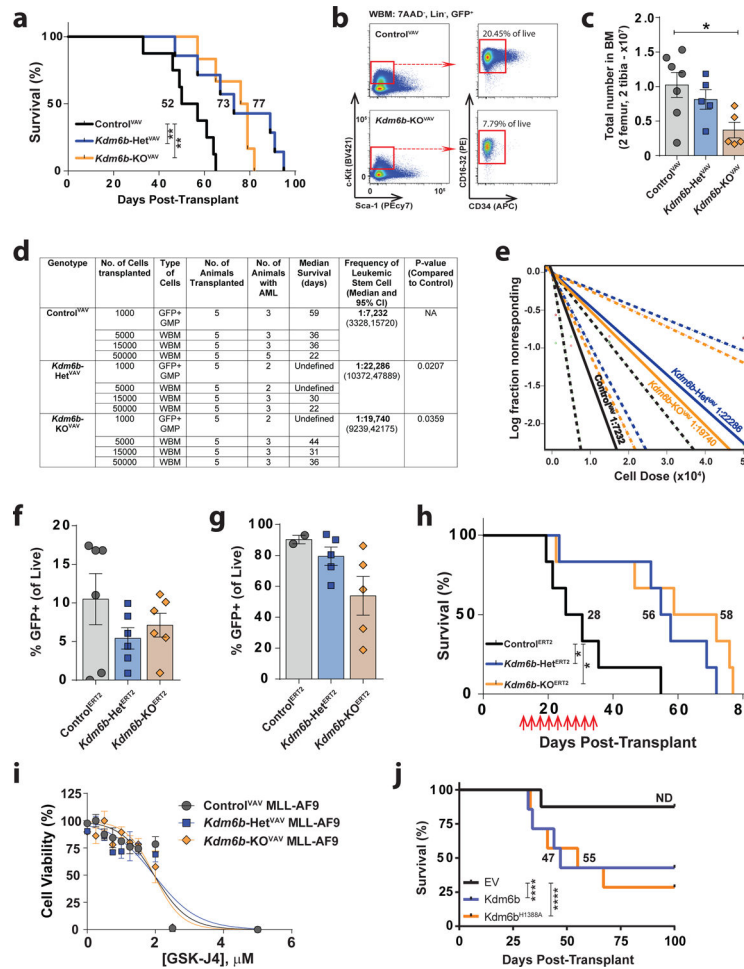


Figure 7: Kdm6b is required for self-renewal of MLL-AF9 leukemia-initiating cells. (a) Kaplan-Meier plot comparing time to morbidity between mice transplanted with Control^{VAV} ($n=8$), *Kdm6b*-Het^{VAV} ($n=7$), and *Kdm6b*-KO^{VAV} ($n=6$) c-Kit⁺ BM cells transduced with MLL-AF9. (b) Representative flow cytometry plots showing leukemia-initiating cells (GFP⁺ GMPs) in MLL-AF9 Control^{VAV} (top) and *Kdm6b*-KO^{VAV} (bottom) recipient mouse BM. (c) Absolute number of leukemic GMPs in BM of moribund recipient mice. (d) Secondary limiting dilution transplantation response from transfer of stated doses of cells from primary moribund animals. (e) Leukemic-initiating cell frequency estimates calculated by ELDA software. (f) Frequency of GFP⁺ cells in blood of mice transplanted with Control^{ERT2}, *Kdm6b*-Het^{ERT2}, and *Kdm6b*-KO^{ERT2} c-Kit⁺ BM cells transduced with MLL-AF9 two-weeks post-transplant. (g) Frequency of GFP⁺ cells in blood of surviving mice transplanted with MLL-AF9-expressing cells two-days post-tamoxifen treatment. (h) Kaplan-Meier plot comparing time to morbidity between mice transplanted with Control^{ERT2} ($n=6$), *Kdm6b*-Het^{ERT2} ($n=6$), and *Kdm6b*-KO^{ERT2} ($n=6$) c-Kit⁺ BM cells transduced with MLL-AF9. Red arrows indicate timing of tamoxifen injections. (i) Dose response of Control^{VAV}, *Kdm6b*-Het^{VAV} and *Kdm6b*-KO^{VAV} MLL-AF9 AML cells to increasing concentrations of GSK-J4 ($n=3$). (j) Kaplan-Meier plot comparing time to morbidity between mice transplanted with *Kdm6b*-KO^{VAV} MLL-AF9 AML cells transduced

with lentiviruses expressing *Kdm6b*, *Kdm6b*^{H1388A}, or empty vector (EV) control ($n=7$ recipient mice, $n=3$ independent AMLs). * $p<0.05$, ** $p<0.01$. Mean \pm S.E.M. values are shown.

Author Manuscript

Author Manuscript

Author Manuscript

Author Manuscript

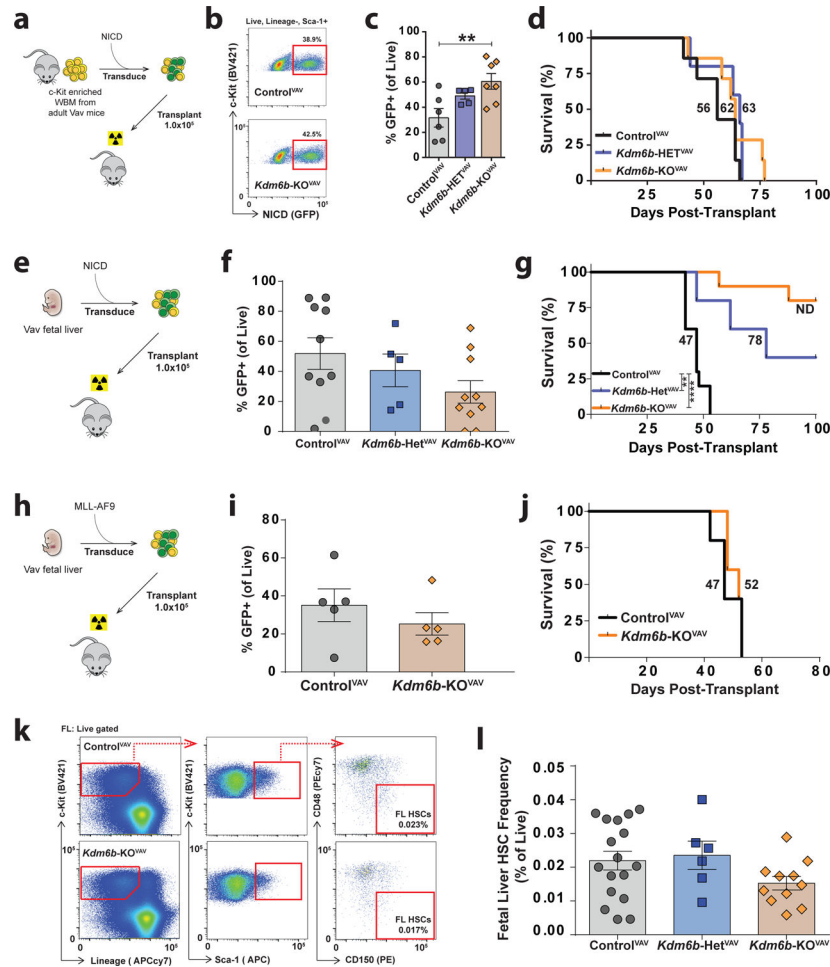


Figure 8: *Kdm6b* supports context-dependent leukemogenesis.

(a) Schematic for transduction of adult c-Kit⁺ BM progenitors with NICD virus and transplantation. (b) Representative flow cytometry plots showing NICD transduction efficiencies in Lineage- c-Kit⁺ Sca-1⁺ cells 48-hours post-transduction. (c) Frequency of NICD-GFP⁺ cells in peripheral blood of recipient mice four-weeks post-transplant of adult BM progenitor cells. (d) Kaplan-Meier plot comparing time to morbidity between mice transplanted with Control^{VAV} (*n*=7), *Kdm6b*-HET^{VAV} (*n*=5) and *Kdm6b*-KO^{VAV} (*n*=7) adult c-Kit⁺ cells transduced with NICD. (e) Schematic for transduction of fetal liver c-Kit⁺ progenitors with NICD virus and transplantation. (f) Frequency of NICD-GFP⁺ cells in peripheral blood of recipient mice four-weeks post-transplant of fetal liver progenitor cells. (g) Kaplan-Meier plot comparing time to morbidity between mice transplanted with Control^{VAV} (*n*=10), *Kdm6b*-HET^{VAV} (*n*=5) and *Kdm6b*-KO^{VAV} (*n*=10) fetal liver c-Kit⁺ cells transduced with NICD. (h) Schematic for transduction of fetal liver c-Kit⁺ progenitors with MLL-AF9 virus and transplantation. (i) Frequency of MLL-AF9⁺ cells in peripheral blood of recipient mice four-weeks post-transplant of fetal liver progenitor cells. (j) Kaplan-Meier plot comparing time to morbidity between mice transplanted with Control^{VAV} (*n*=5) and *Kdm6b*-KO^{VAV} (*n*=5) fetal liver c-Kit⁺ cells transduced with MLL-AF9. (k) Flow cytometry gating scheme to identify HSCs in E14.5 fetal liver. (l) Quantification of HSC

frequency in Control^{VAV}, *Kdm6b*-HET^{VAV} and *Kdm6b*-KO^{VAV} E14.5 fetal liver. ** $p < 0.01$, *** $p < 0.001$. Mean \pm S.E.M. values are shown.

Author Manuscript

Author Manuscript

Author Manuscript

Author Manuscript